

1 Geophysical evidence for crustal and mantle weak zones
2 controlling intra-plate seismicity – the 2017 Botswana
3 earthquake sequence

4 Max Moorkamp^{a,b}, Stewart Fishwick^a, Richard J. Walker^a, & Alan G.
5 Jones^c

6 ^a School of Geography, Geology and the Environment, University of Leicester, University
7 Road, Leicester LE1 7RH, UK

8 ^b now at: Ludwig-Maximilians-Universität, Department of Earth and Environmental
9 Sciences, Theresienstrasse 41, 80333 Munich, Germany

10 ^c Complete MT Solutions Inc., Ottawa Canada. Formerly Dublin Institute for Advanced
11 Studies, Dublin, Ireland

12 **Abstract**

Large earthquakes away from plate boundaries pose a significant threat to human lives and infrastructure, but such events typically occur on previously unknown faults. Most cases of intra-plate seismicity result from compression related to far-field plate boundary stresses. The April 2017 M_W 6.5 earthquake in central Botswana, and subsequent events, occurred in a region with no previously known large earthquakes, occurred away from major present day tectonic activity, and accommodate extension rather than compression. Here, we present results from an integrated geophysical study that suggests the recent earthquakes may be a sign of future activity, controlled by the collocation of a weak upper mantle and weak crustal structure, between otherwise strong Precambrian blocks. Magnetotelluric data highlights Proterozoic continent accretion structure within the region, and shows that recent extension and seismicity occurred along ancient thrust faults within the crust. Our seismic velocity and resistivity models suggest a weak zone in the uppermost mantle, that does not persist to greater depths, and is therefore unlikely to represent mantle upwelling. The Botswana events may therefore be indicative of top-down extension as a response to large scale extensional forces.

Email address: Max.Moorkamp@lmu.de (Max Moorkamp)

13 1. Introduction

14 The 3rd April 2017 Botswana earthquake (moment magnitude, M_W 6.5)
15 was the largest event on the African continent outside the East African Rift
16 System (EARS) for over 80 years (cf [1]) (Figure 1). It was part of a sequence
17 of 15 events with magnitudes up to M_W 5. That sequence lasted for 4 months
18 following the main event, with the final event occurring 200 km away on 12th
19 August 2017. Intra-plate earthquakes require sufficient stress to build-up, with
20 most events attributed to far-field effects of deformation at plate boundaries [2].
21 Given that stable continental lithosphere is rigid and strong, these stresses can
22 be transferred over long distances [3]. Such a model of earthquake generation
23 is compatible with thrusting or strike-slip mechanisms and general horizontal
24 contraction, which is observed in most intra-plate events [4].

25 The Botswana event is different in this respect as its focal mechanism indi-
26 cates normal faulting and extension. However, such a mechanism is consistent
27 with stress and stress-gradient calculations for southern Africa [5, 6] which indi-
28 cate large scale extension. Controls on the precise locations of intra-plate events
29 remain debated. Tectonic controls, such as gradients in lithospheric thickness
30 and the presence of weak zones may facilitate movement [7]. For example,
31 earthquakes in the New Madrid Seismic Zone, USA, are thought to be asso-
32 ciated with pre-existing faults and possibly a weak mantle below [8]. Recent
33 work suggests that these large scale factors determine the style of faulting and
34 the stress release, while transient events, possibly due to non-tectonic forces,
35 are responsible for triggering the earthquake [9]. For the Botswana earthquake
36 it has been hypothesized that fluid leaks from the upper mantle have triggered
37 the event [10].

38 Although Botswana does not show any strong earthquakes in instrumented
39 history, the clustering of small magnitude events in the Okavango delta in north-
40 ern Botswana has led to speculation of an incipient rift [13] - the Okavango Rift
41 Zone (ORZ) [14] - which may represent the southwestern continuation of the
42 EARS [15]. Most of the current understanding of the deeper crustal and upper

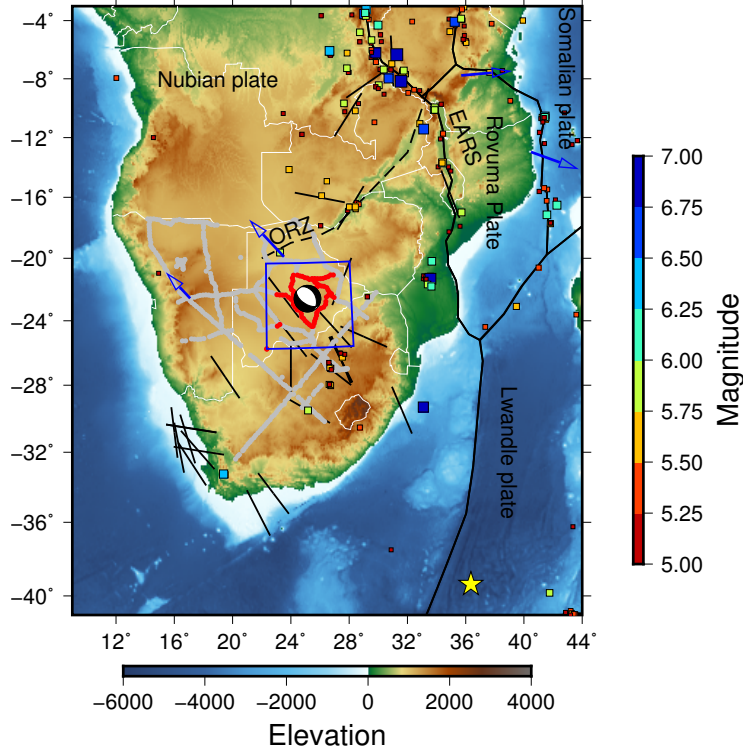


Figure 1: Map of southern and central Africa. The study area is shown with a blue rectangle and we show the location and focal mechanism of the 03/04/2017 earthquake. Black lines show plate boundaries whereas the dashed line indicates the proposed south-western continuation of the East African Rift System (EARS) to the Okavango Rift Zone (ORZ). Colored boxes show all seismic events in the USGS earthquake catalogue with moment magnitude > 5 , where color and size indicate magnitude. Black bars indicate maximum horizontal stress direction from the World Stress Map[11]. Blue arrows show inferred plate motion with respect to the Nubian plate[12] and the yellow star marks the Euler pole for the Somalia-Nubia plate motion. The locations of the SAMTEX MT sites are shown in grey and red circles, where the red ones are modelled in this paper.

mantle structures in the region is based on a profile of magnetotelluric (MT) data to the east [16], and inversion of receiver functions [17], shear wave splitting analysis [18], and seismic tomography [15] along the profile of the SAFARI experiment. Potential field data have been used to identify the boundaries between different tectonic units [14, 19], but significant uncertainty remains as to the location and nature of those units (compare [14, 16, 18, 20, 21]).

2. Inverting magnetotelluric and surface wave data

Here we present 3D models of the lithosphere south of the ORZ and centered on the April 2017 event, based on MT measurements (e.g. [22]) and regional surface wave data. We use magnetotelluric transfer functions from 81 stations in the vicinity of the hypocentre (Figure 1) from the publicly available SAMTEX dataset[23], and invert them using the 3D inversion methodology described in [24] that includes correction for static distortion [25]. We select data at 24 periods between 1 s and 600 s corresponding to depths between 5 km and 80km as confirmed by sensitivity tests (see supplementary material). We start the inversion with a high smoothing regularization term to recover the broad conductivity structure and successively lower the weight of the regularization until we achieve an adequate fit to the observed data. The final inversion model (Figures 2 and 3) explains the data to a RMS of 1.3 assuming an error floor of 2% of the Berdichevsky invariant of the impedances. This choice of error floor down-weights small diagonal elements in the inversion, but has the advantage of making the misfit rotationally invariant. Still we observe an excellent fit to all elements of the impedance tensor.

Figure 4 shows a representative selection of magnetotelluric data and the associated model fits. Stations 24 and 25 (top row in Figure 4) are located closest to the epicentre of the 3rd April event and show excellent fit for all components across the whole frequency range. Station 5 (bottom left in Figure 4) is located close to the 12th August event and shows a good fit for all components and frequencies. Station 79 (bottom right in Figure 4) is the site with highest

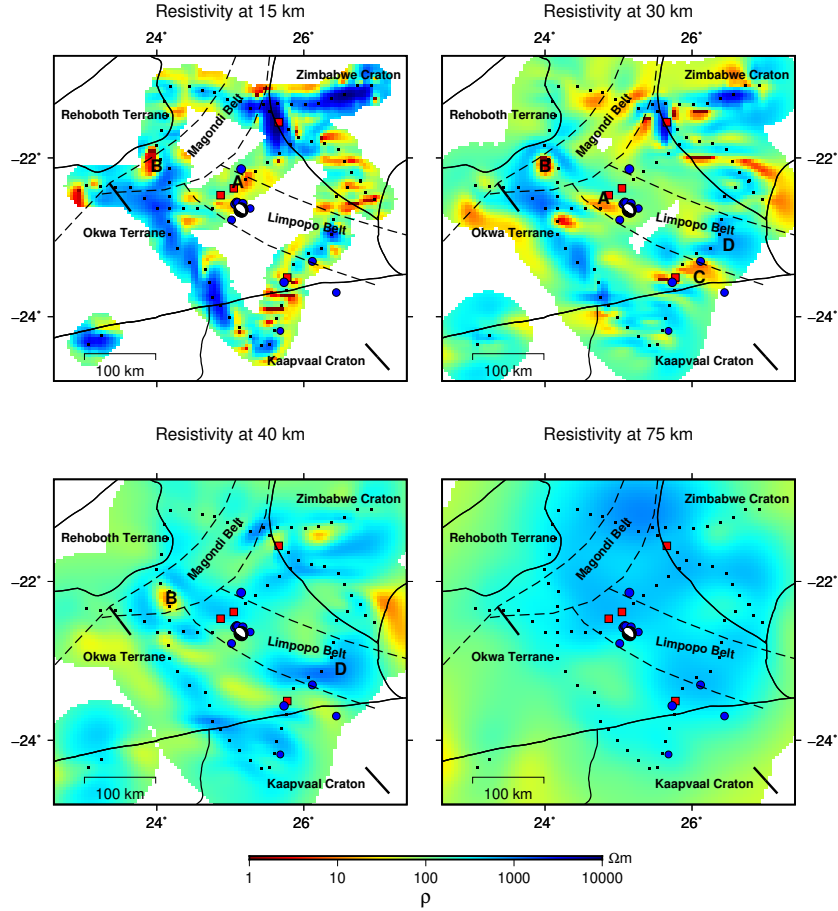


Figure 2: Horizontal slices through our preferred resistivity model. The magnetotelluric stations used in the inversion are marked as black squares. We show the location and focal mechanism of the April recent earthquake as well as the location of seismicity in the area (blue dots) and the August 2017 magnitude 5 event (red dot). Solid black lines show the boundaries of tectonic units with additional crustal units from [26] (dashed lines). Thick black bars show the direction of maximum horizontal stress from the world stress map[11].

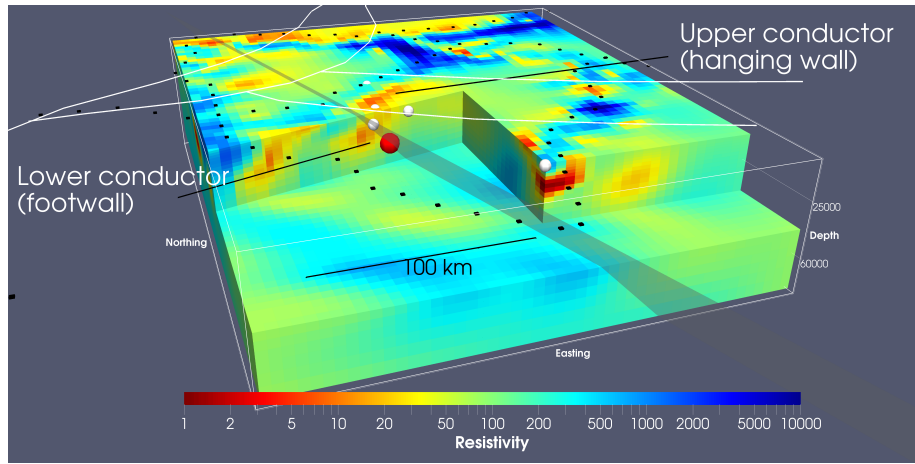


Figure 3: Cut through the preferred resistivity model viewed from the South-West. MT measurement site locations are marked by black squares and the location of the hypocentres are marked by dots. The main April 2017 event is marked in red and subsequent events in white. For the main event we plot the preferred fault plane from the moment tensor solution and D-InSAR modelling [27] as a transparent plane. The white lines mark the boundaries of major crustal units [26]

72 RMS misfit of all sites considered in the inversion. Note that the apparent
73 resistivities of the two off-diagonal components of impedance differ by two orders
74 of magnitude, an indication of strong static distortion. Despite this, we achieve a
75 reasonable fit to the observed data even though some of the more subtle features
76 are not reproduced by the model.

77 The surface wave inversion uses a two stage approach to generate the to-
78 mographic models similar to the methodology outlined in [28]. The Rayleigh
79 wave portion of the seismograms (periods of 50 - 120 s) are inverted to find the
80 average 1D shear (S_v) velocity structure between source and receiver. In the ap-
81 proach taken here, for each waveform inversion four different starting models are
82 used that incorporate prior information on crustal, and long wavelength man-
83 tle structure (see e.g., [28]). A particular advantage of incorporating the prior
84 mantle structure in the starting models is that for the upper mantle there are
85 significant differences between the general structure of oceans and continents.
86 Using a 1D radially averaged starting model (such as PREM or ak135) will limit
87 the recovery of the amplitude of anomalies beneath the different regions due to
88 the necessary regularisation in the waveform inversion.

89 The resulting 1D velocity models are then combined to produce tomographic
90 images, as a series of depth slices at 25 km intervals, of the lateral velocity vari-
91 ations within the upper mantle. To improve the reliability of these tomographic
92 models, data from closely adjacent paths are clustered, this has the benefit of
93 limiting the impact of 1D models that are not consistent with adjacent results,
94 and somewhat downweighting areas that would be dominated by path coverage
95 in one particular direction. For the recovery of the variations in velocity there
96 are two steps in the inversion. Initially, a strongly damped inversion using over
97 $> 45,000$ 1D models, is performed to recover the longest wavelength structure.
98 Subsequently, the tomographic model is updated through an inversion using
99 a parameterisation with knot points at 3-degree intervals. This intermediate
100 stage provides good recovery of structures such as the mid ocean ridges and
101 subduction zones, and therefore minimises the potential for these velocity fea-
102 tures to be smeared into the final model. For the final inversion focused on

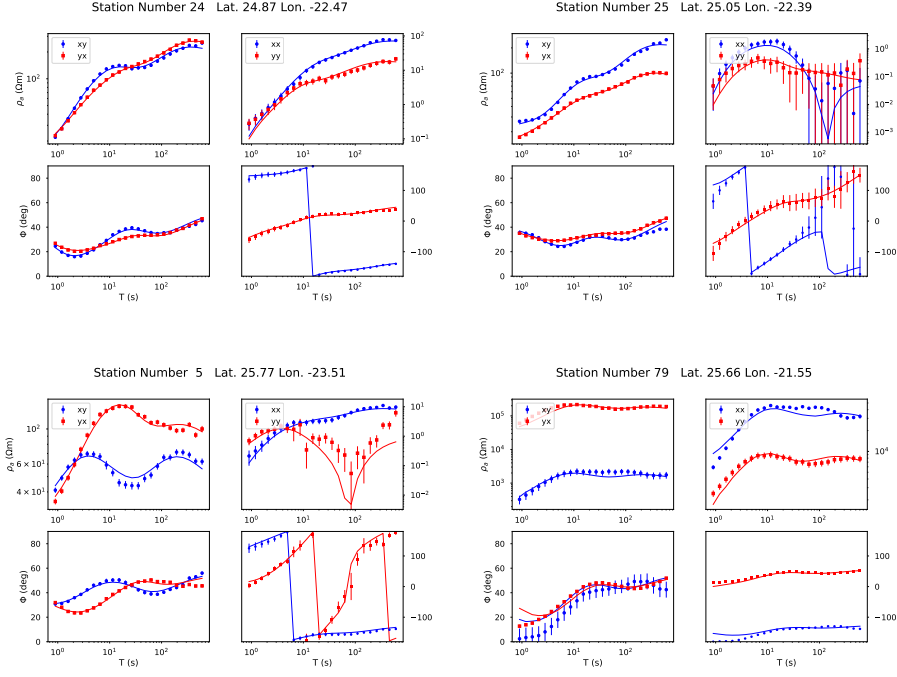


Figure 4: The fit of the final conductivity model for four selected MT sites. Stations 24 and 25 (top row) are the two stations closest to the main event. Station 5 (bottom left) is the MT site closest to the August 12th event. Station 79 (bottom right) has the highest misfit of all inverted MT stations. These sites are marked by red squares in Figure 2.

103 southern and east Africa a subset of paths is included, quantile-quantile plots
 104 are used to remove outliers (further limiting the impact of data that cannot be
 105 fit in the inversion procedure), and almost 19,500 paths are incorporated into
 106 the tomography (see Figure 5). The final models for each depth slice are chosen
 107 based on the trade off between data fit and a model norm regularisation. In this
 108 approach to regularisation, the specific choice of damping has an impact on the
 109 amplitude of the velocity anomalies, however the spatial location of variations in
 110 velocity in the resulting models remain consistent. Checkerboard tests illustrate
 111 that the path coverage in the region is sufficient to recover structures around
 112 300 km in diameter with limited smearing (see Supplementary Information for
 113 associated figures).

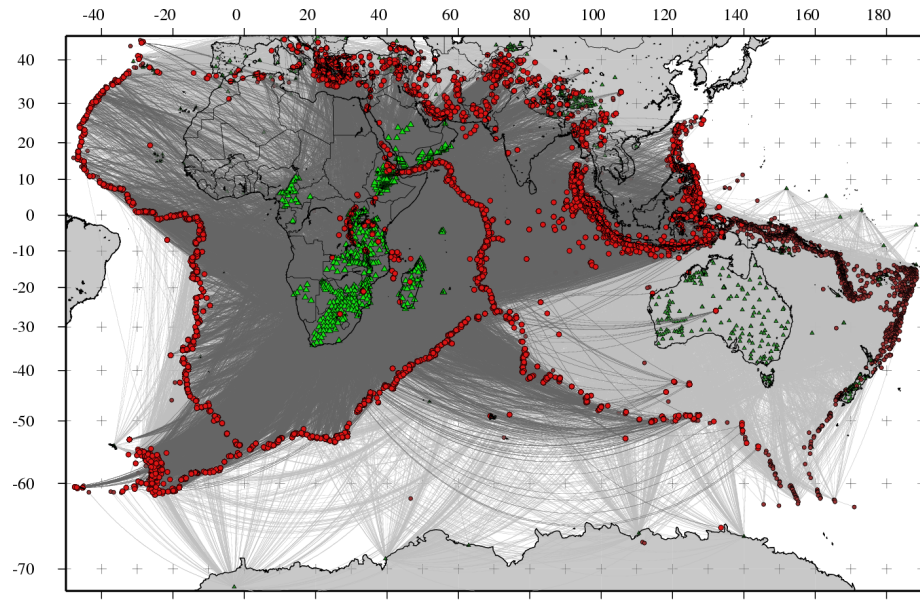


Figure 5: Events (red circles), stations (triangles) and path coverage (gray lines) used to construct the seismic surface wave model. The light gray paths show the coverage for the large scale model which is used as starting model for the regional model shown here. Dark gray paths indicate coverage for the final regional model.

114 3. Crustal structure

115 Given the heterogeneous data coverage with the MT sites located on profiles
116 along accessible roads, we focus our discussion of the resistivity model on struc-
117 tures close to these profiles. Our sensitivity tests demonstrate though that we
118 have some sensitivity to off-profile structures (see Supplementary material). We
119 estimate that we can recover structures up 1.5 skin depths in lateral direction
120 and blank the areas in Figure 2 where we do not have sensitivity.

121 At depths between 15 km and 40 km, most of the significant conductors
122 (resistivity $\rho < 25 \Omega\text{m}$) terminate at geological boundaries (Figure 2). This is
123 particularly evident for anomalies A, B, and C, but other conductive structures
124 also show the same pattern. Resistive structure D, which emerges at a depth of
125 30-40 km, is bound on both sides by the inferred boundaries of the Proterozoic-
126 age Limpopo Belt. We note that the hypocentres of all seismic events in the
127 region are located at the boundary of conductive structures (see Figures 3 and
128 6).

129 Conductors in the middle and lower crust can have a variety of origins de-
130 pending on the geological setting. In strongly tectonically active areas they have
131 been interpreted as accumulations of melt [e.g. 29]. This requires an unusually
132 hot crust and thus can be ruled out in a stable continental setting. In such
133 regions, enhanced conductivities at depths between 10 and 30 km are typically
134 attributed to relatively small amounts of saline fluids [e.g. 30] or interconnected
135 graphite and, to a lesser degree, sulphides [e.g. 31].

136 Regardless of which of these processes are considered, they all require the
137 conductive phase to be interconnected over distances of several kilometres in or-
138 der to cause an observable increase in conductivity. For graphite and sulphides,
139 the simplest geological process to achieve such interconnectivity is deformation
140 along shear zones creating thin boundary films [32]. Consequently many con-
141 ductivity anomalies in the middle to lower crust have been interpreted as signs
142 of significant deformation, particularly when there is strong variation in depth
143 to the conductor [16, 31, 33, 34, 35]. Where fluids are considered to be the

144 cause of enhanced conductivity, they are often thought to be trapped under
 145 an impermeable layer in the middle crust [36]. Large faults can breach such a
 146 seal and allow fluids to migrate upwards. This explanation has been invoked
 147 to explain the observed conductivities of major active fault systems such as the
 148 San Andreas Fault (SAF) [37, 38]. At the SAF, a deep (30-60 km) conductor is
 149 interpreted as a fluid reservoir that feeds a more shallow fault related fracture
 150 zone imaged as a narrow vertical conductor. Similar images and interpreta-
 151 tions have been obtained in other active fault zones, e.g. the North Anatolian
 152 fault and the Niigata-Kobe Tectonic Zone in Japan [38]. In regions without sig-
 153 nificant ongoing tectonic activities, interconnected graphite is usually favoured
 154 as an explanation for fault related conductivity as fluids migrate upwards over
 155 geological time scales [33] and the deep conductor found in active regions ap-
 156 pears to be missing. However, fluids can assist in transporting graphite during
 157 deformation and contribute to the formation of connected films [33].

158 Of particular interest for our study is the conductive structure associated
 159 with the hypocentre of the main event. Figure 3 shows a 3D cutout view of the
 160 preferred resistivity model together with the preferred fault plane solution based
 161 on the moment tensor, and the Differential Interferometric Synthetic Aperture
 162 Radar modelling of [27]. The inferred fault plane coincides with a significant
 163 change in depth of the crustal conductor in this area. In the foot wall on the
 164 western side its top is located at a depth of 14 km, whereas in the hanging wall to
 165 the east, the conductor reaches the surface. Sensitivity tests (see supplementary
 166 material) demonstrate that we have good resolution to the depth of the deep
 167 conductor, and that the top on the eastern side cannot be located deeper than
 168 7 km.

169 Considering the above discussion of causes for high conductivity in fault
 170 zones, these structures could be a direct expression of fault related deforma-
 171 tion or could be an originally continuous structure that has been displaced by
 172 movement on the fault. Given the spacing between the MT sites (20 km), we
 173 cannot directly image the fault zone, which is at most hundreds of meters wide.
 174 Instead we image the effect of the fault on the surrounding structures. Based

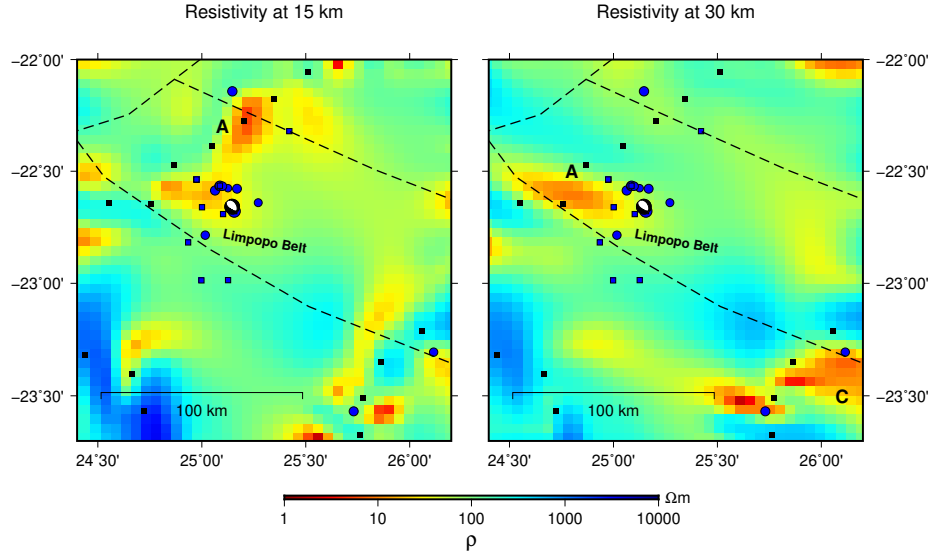


Figure 6: Magnified view of the model shown in Figure 2 around the earthquake sequence. The magnetotelluric stations in the area are marked as black squares. We show the location and focal mechanism of the April recent earthquake as well as the locations of seismicity in the area from the USGS catalogue (blue dots), the precursor locations determined in [10] (blue squares).

on the published estimates of the geometry of the fault for this event [27, 10], it is unlikely that we are imaging fluid pathways or shear signatures caused by the currently active fault. Instead it is more plausible that the two conductors were originally at the same depth and subsequently displaced by movement along the fault. However, the sense of motion necessary to produce such a displacement is opposite to the observed current fault motion. Thus our preferred interpretation is that the earthquake reactivated an existing thrust fault associated with the deformation associated with the collision of the Kaapvaal and Zimbabwe Cratons. This interpretation is consistent with other observations [27] and similar interpretations have been made for other paleo-faults [34].

The reactivation of an existing fault fits well with other studies of intra-plate earthquake nucleation [8]. However, the question remains to which degree the mid-crustal event corresponds also to deeper regional structure? In particular,

188 can we identify a fluid reservoir that corroborates the hypothesis that this event
 189 was triggered by fluid released from the mantle [10]?

190 4. Upper mantle structure

191 In the context of deeper regional structure, Figure 7 shows the S_v velocity
 192 for the region of southern Africa at depths of 75 km and 175 km (top row)
 193 and for the study area (bottom row), together with heat flow measurements
 194 [39], the directions of maximum horizontal stress [11] and relative plate motion
 195 from GPS data [12]. At 75 km depth the areas of the Kaapvaal and Zimbabwe
 196 cratons are clearly marked by high velocities ($v_s > 4.6$ km/s), as expected for
 197 cold cratonic mantle. Similar fast velocities are observed beneath other areas of
 198 Archean age, e.g., the Tanzanian Craton, and fragments of the Congo Craton
 199 such as the Kazai shield. In the vicinity of the Botswanan earthquake we ob-
 200 serve a low velocity structure ($v_s \approx 4.4$ km/s) at 75 km trending NW-SE and
 201 with a velocity minimum in the region of the earthquake. In contrast, at 175 km
 202 depth, fast velocities ($v_s > 4.6$ km/s) typical of thick continental lithosphere are
 203 observed across a broader region of much of southeastern Botswana consistent
 204 with features observed in global tomographic models [40]. While low velocity
 205 zones in the upper mantle can represent zones of high temperature, and po-
 206 tentially partial melting, the underlying faster velocities make this explanation
 207 untenable. Although the heat flow measurements are moderately high (40-60
 208 mW/m²) away from the Kaapvaal and Zimbabwe Cratons [39, 41], the spatial
 209 variability and lack of correlation with velocities at 175 km depth, suggest a pre-
 210 dominate crustal control on heat flow rather than variations due to lithospheric
 211 thickness.

212 Examining our resistivity model between 40 and 75 km (Figure 2), we see
 213 that the deep parts are generally resistive at depth with most parts exceeding
 214 resistivities of 500 Ω m. Based on sensitivity tests (Supplementary material), we
 215 conclude that our data do not indicate a significant difference in resistivity be-
 216 tween the Limpopo Belt and the surrounding Cratons at this depth and assume

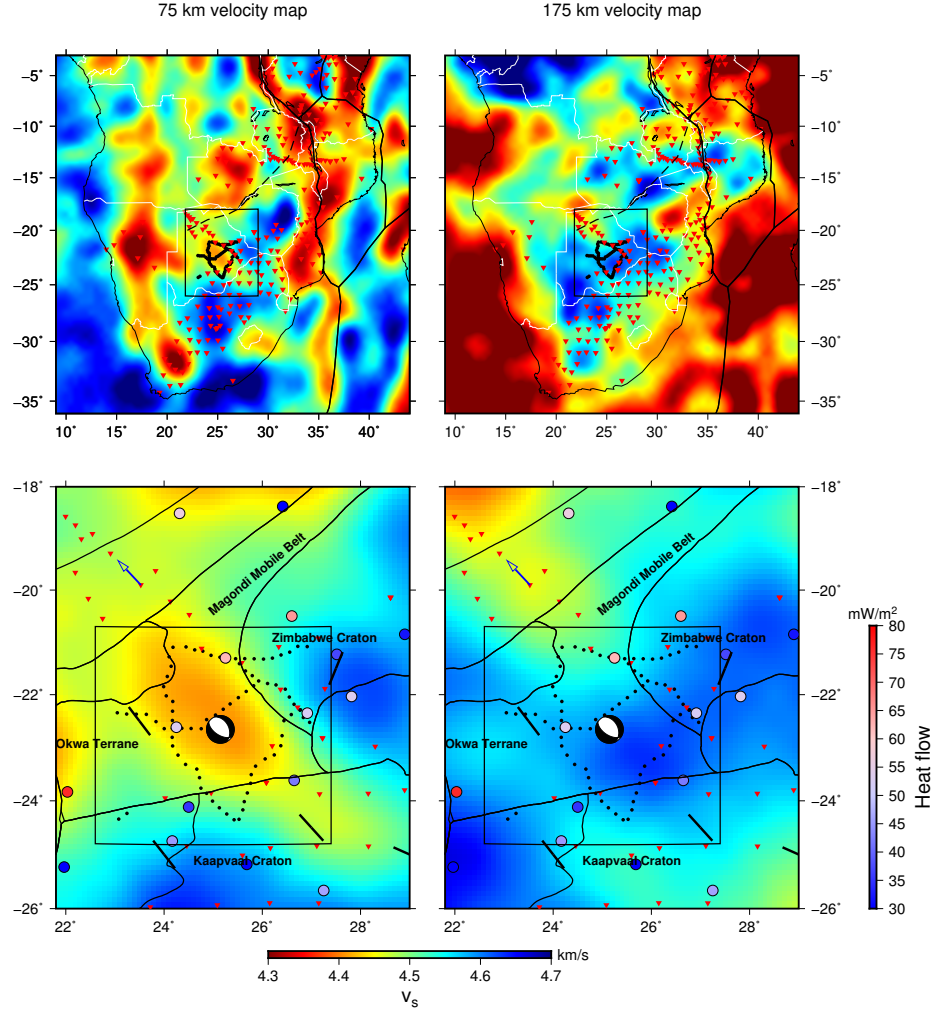


Figure 7: Horizontal slices through our regional surface wave model at depths of 75 km and 175 km, respectively. The top row shows the wider southern African context, while the bottom row shows the region around the earthquake. In addition to stress orientations [11] (black bars), we also show the movement relative to the Nubian plate [12] (blue arrow) and heat flow measurements [39] (coloured dots) in the area. The seismic stations in the plotted area are shown as red triangles.

217 values of 200 –1000 Ωm as representative. Similar resistivities at these depths
218 have also been observed in studies of the surrounding areas [16].

219 Dry Archean lithospheric mantle is expected to show resistivities in excess of
220 10,000 Ωm based on laboratory experiments within the typical compositional
221 variations between Lherzolite and Harzburgite [23]. Such high resistivities are
222 observed at the cores of the Kaapvaal Craton [42] and Congo Craton [16] at
223 depths between 100-200 km, and in parts of the Slave Craton [43]. These high
224 resistivity areas also show S-wave velocities exceeding 4.6 km/s in the seismic
225 velocity model as expected for old lithosphere. The resistivity values we observe
226 cannot be explained by a dry mantle, but match the range of resistivities of 500-
227 2000 Ωm estimated at this depth for typical mantle compositions with a water
228 content of 150 ppm [44]. Such a water content agrees well with the estimated
229 average water content of the lithospheric mantle [45]. Calculations of S-wave
230 velocity for a range of compositions and temperature profiles predict values
231 in excess of 4.5 km/s at a depth of 80 km [46] which matches the values we
232 observe towards the south, in the Kaapvaal Craton, but is significantly higher
233 than the velocities recovered around the epicentre. So, while the resistivity
234 model indicates a relatively homogeneous, normal lithospheric mantle structure,
235 the seismic model requires a strong change in physical properties between the
236 cratons in the south and the region of the epicentre.

237 5. Discussion and conclusions

238 It has been suggested that the event was triggered by fluid release from the
239 mantle bringing a critically loaded fault network to failure [10]. The crustal
240 structure in our resistivity model is compatible with such a scenario. As ex-
241 plained above, we cannot directly image the fault zone as this would require
242 denser site spacing near the fault and higher frequency data than what is cur-
243 rently available. The two displaced conductive structures could be fluid related
244 although this would require some form of seal to prevent those fluids from mi-
245 grating upwards. For this reason we consider an explanation in terms of graphite

246 more likely. Even if the high conductivity in the crust is at least partially caused
247 by saline fluids, these structures cannot be the source for the fluid pulse that
248 triggered the event, as the epicentre is located below these conductors at the
249 transition to more resistive material.

250 A major region of elevated fluid content in the mantle would manifest itself
251 as a region of high conductivity [37]. We do not see such structures in our model.
252 In fact, the lack of strong variation in resistivity in the upper mantle underneath
253 the study area, suggests a homogeneous thermal structure and water content
254 as these are the two major controlling factors on resistivity in the nominally
255 anhydrous minerals (NAMs) of the lithosphere [47]. Therefore, either the source
256 region of the fluids is spatially restricted (less than a few kilometres in diameter),
257 the fluids are derived from moderate amounts of ambient water in the mantle or
258 another triggering mechanism is responsible. Based on our results, we cannot
259 distinguish between these alternatives. Thus, although our model does not show
260 the expected features of a mantle fluid reservoir, we cannot refute the hypothesis
261 put forward by [10].

262 We will now focus the discussion on the potential origins of the low velocity
263 zone at 80 km depth. Variations in temperature or water content would result
264 in observable resistivity variations [47]. We can therefore exclude these two
265 variables as an explanation for the low velocities. Furthermore, both have a
266 similar effect on resistivity and seismic velocity and thus an increase in temper-
267 ature accompanied by a decrease in water content or vice versa is not feasible
268 either. This leaves two possible explanations for a decrease in velocity that is
269 not accompanied by a change in resistivity: i) Variations in mantle composition
270 and ii) variations in grain size of olivine. A bulk compositional change compat-
271 ible with our observations would have to maintain iron content (or equivalently
272 Magnesium number: $Mg\#$) as variations in $Mg\#$ have observable effects on
273 conductivity [23].

274 Compositional explanations for low velocities in the uppermost lithosphere
275 have been discussed previously. [48] suggested qualitatively that paragonitic am-
276 phiboles could contribute to lowering velocities in central Australia, in a region

277 of thick lithosphere, but noted that this would require a complicated layered
 278 structure with no clear mechanism of formation. The presence of chrome, thus
 279 lowering the depth of the spinel transition, has been invoked as a possible expla-
 280 nation for the velocity gradients seen in Precambrian lithosphere of a number
 281 of areas [49]. Modelling of phase velocity profiles for cratonic regions also indi-
 282 cated that models of constant composition have a systematic variation from the
 283 seismic data [50] and further studies using these data indicate that a metaso-
 284 matic component (water or carbonate fluids) improve the fit to the seismological
 285 observations [51]. However, the velocity variations observed in our study region
 286 have larger variations than those modelled in [51].

287 The idea of enhanced concentrations of amphibole, has been revisited, and
 288 invoked to explain low velocities at a similar depth range and magnitude in-
 289 ferred from S-receiver functions [52]. The electrical resistivity of amphiboles
 290 at upper mantle conditions is currently unclear, but laboratory measurements
 291 under lower crustal conditions suggest a significant decrease in resistivity from
 292 amphibole enrichment [53]. We therefore cannot rule out amphibole as a source
 293 of the observed low velocities, but consider the high concentrations ($\sim 20\%$) in-
 294 voked by [52] to explain a similar magnitude low velocity anomaly improbable.

295 Variations in grain size have been shown to affect seismic velocities in the
 296 mantle and a reduction in size from approximately 1 cm below the cratons
 297 to several millimeters below the mobile belt is sufficient to explain the lower
 298 seismic velocities below the Limpopo mobile belt [54]. Such sizes are consistent
 299 with estimated values in undeformed cratonic lithosphere and deformed mobile
 300 belts, respectively [55]. Electrical resistivity shows dependence on grain size
 301 for sizes below 1 mm, but for the range of sizes considered here is negligible
 302 [47]. Deformation can result in a grain size reduction in the upper mantle
 303 that can persist for several hundred million years [56]. Thus we consider a
 304 reduced grain size below the Limpopo belt the most likely explanation for our
 305 observations. Interestingly, our two most likely explanations, reduced grain size
 306 and amphibole enrichment are typically observed in samples from mantle shear
 307 zones[57]. Furthermore, a reduced grain size results in a reduced viscosity [55]

308 indicating that the low velocity zone underneath the Botswana earthquake is
309 an expression of a weak mantle.

310 Our combined magnetotelluric and seismic study demonstrates that the re-
311 cent Botswana earthquake sequence reactivated previous faults in the area. For
312 the main event, this reactivation occurs in the opposite sense to the original
313 fault movement. All events occur above a region of low velocities and relatively
314 high resistivities in the upper-most mantle that we interpret as a region of re-
315 duced grain size and thus weaker material compared to its surroundings. The
316 observed extensional fault movement is compatible with the ambient stress pat-
317 tern in southern Africa. Our results can neither confirm nor refute the proposed
318 triggering of the event by mantle derived fluids. We do however see signs of a rhe-
319 ologically weak upper mantle. The lack of a significant deep lithospheric thermal
320 anomaly then suggests that this process is initiated from the top, through inter-
321 action of the ambient stress field with ancient structures, rather than through
322 thermal weakening from below.

- 323 [1] F. Krüger, F. Scherbaum, The 29 September 1969, Ceres, South Africa,
324 earthquake: Full waveform moment tensor inversion for point source and
325 kinematic source parameters, *Bulletin of the Seismological Society of Amer-*
326 *ica* 104 (1) (2014) 576–581.
- 327 [2] P. Talwani, The intersection model for intraplate earthquakes, *Seismologi-*
328 *cal Research Letters* 59 (4) (1988) 305–310.
- 329 [3] L. R. Sykes, M. L. Sbar, Intraplate earthquakes, lithospheric stresses and
330 the driving mechanism of plate tectonics, *Nature* 245 (5424) (1973) 298–
331 302.
- 332 [4] D. E. McNamara, H. M. Benz, R. B. Herrmann, E. A. Bergman, P. Earle,
333 A. Holland, R. Baldwin, A. Gassner, Earthquake hypocenters and focal
334 mechanisms in central Oklahoma reveal a complex system of reactivated
335 subsurface strike-slip faulting, *Geophysical Research Letters* 42 (8) (2015)
336 2742–2749.

- 337 [5] D. D. Coblenz, M. Sandiford, Tectonic stresses in the african plate: Con-
338 straints on the ambient lithospheric stress state, *Geology* 22 (9) (1994)
339 831–834.
- 340 [6] D. Stamps, L. Flesch, E. Calais, Lithospheric buoyancy forces in africa
341 from a thin sheet approach, *International Journal of Earth Sciences* 99 (7)
342 (2010) 1525–1533.
- 343 [7] W. D. Mooney, J. Ritsema, Y. K. Hwang, Crustal seismicity and the earth-
344 quake catalog maximum moment magnitude (m_{cmax}) in stable continen-
345 tal regions (scrs): Correlation with the seismic velocity of the lithosphere,
346 *Earth and planetary science letters* 357 (2012) 78–83.
- 347 [8] S. J. Kenner, P. Segall, A mechanical model for intraplate earthquakes:
348 Application to the New Madrid seismic zone, *Science* 289 (5488) (2000)
349 2329–2332.
- 350 [9] E. Calais, T. Camelbeeck, S. Stein, M. Liu, T. Craig, A new paradigm
351 for large earthquakes in stable continental plate interiors, *Geophysical Re-*
352 *search Letters* 43 (20).
- 353 [10] B. Gardonio, R. Jolivet, E. Calais, H. Leclère, The April 2017 Mw6. 5
354 Botswana earthquake: An intraplate event triggered by deep fluids, *Geo-*
355 *physical Research Letters*.
- 356 [11] O. Heidbach, M. Rajabi, K. Reiter, M. Ziegler, W. Team, World stress
357 map database release 2016, Tech. rep., GFZ Data Services (2016).
358 doi:10.5880/WSM.2016.001.
359 URL <http://doi.org/10.5880/WSM.2016.001>
- 360 [12] E. Saria, E. Calais, Z. Altamimi, P. Willis, H. Farah, A new velocity field
361 for Africa from combined GPS and DORIS space geodetic solutions: Con-
362 tribution to the definition of the African reference frame (AFREF), *Journal*
363 *of Geophysical Research: Solid Earth* 118 (4) (2013) 1677–1697.

- [13] C. Reeves, Rifting in the Kalahari?, *Nature* 237 (5350) (1972) 95–96.
- [14] K. Leseane, E. A. Atekwana, K. L. Mickus, M. G. Abdelsalam, E. M. Shemang, E. A. Atekwana, Thermal perturbations beneath the incipient Okavango Rift zone, northwest Botswana, *Journal of Geophysical Research: Solid Earth* 120 (2) (2015) 1210–1228, 2014JB011029. doi:10.1002/2014JB011029.
- [15] Y. Yu, K. H. Liu, Z. Huang, D. Zhao, C. A. Reed, M. Moidaki, J. Lei, S. S. Gao, Mantle structure beneath the incipient Okavango rift zone in southern Africa, *Geosphere* 13 (1) (2017) 102–111.
- [16] T. D. Khoza, A. G. Jones, M. R. Muller, R. L. Evans, M. P. Mienso-pust, S. J. Webb, Lithospheric structure of an Archean craton and adjacent mobile belt revealed from 2-D and 3-D inversion of magnetotelluric data: Example from southern Congo Craton in northern Namibia, *Journal of Geophysical Research: Solid Earth* 118 (8) (2013) 4378–4397.
- [17] Y. Yu, K. H. Liu, M. Moidaki, C. A. Reed, S. S. Gao, No thermal anomalies in the mantle transition zone beneath an incipient continental rift: evidence from the first receiver function study across the Okavango rift zone, botswana, *Geophysical Journal International* 202 (2) (2015) 1407–1418.
- [18] Y. Yu, S. S. Gao, M. Moidaki, C. A. Reed, K. H. Liu, Seismic anisotropy beneath the incipient Okavango rift: Implications for rifting initiation, *Earth and Planetary Science Letters* 430 (2015) 1–8.
- [19] R. Ranganai, A. Kampunzu, E. Atekwana, B. Paya, J. King, D. Koosimile, E. Stettler, Gravity evidence for a larger Limpopo Belt in southern Africa and geodynamic implications, *Geophysical Journal International* 149 (3) (2002) F9–F14.
- [20] A.-M. Pastier, O. Dauteuil, M. Murray-Hudson, F. Moreau, A. Walpersdorf, K. Makati, Is the Okavango delta the terminus of the East African Rift System? towards a new geodynamic model: *Geodetic*

- study and geophysical review, *Tectonophysics* 712 (2017) 469 – 481.
doi:<http://dx.doi.org/10.1016/j.tecto.2017.05.035>.
- [21] I. Fadel, M. van der Meijde, H. Paulssen, Crustal structure and dynamics of Botswana, *Journal of Geophysical Research: Solid Earth* accepted (ja).
doi:10.1029/2018JB016190.
- [22] A. Jones, S. Fishwick, R. Evans, M. Muller, J. Fulla, Velocity-conductivity relations for cratonic lithosphere and their application: Example of Southern Africa, *Geochemistry, Geophysics, Geosystems* 14 (4) (2013) 806–827.
- [23] A. G. Jones, R. L. Evans, M. R. Muller, M. P. Hamilton, M. P. Mienso-
pust, X. Garcia, P. Cole, T. Ngwisanyi, D. Hutchins, C. Fourie, H. Jelsma,
S. Evans, T. Aravanis, W. Pettit, S. Webb, J. Wasborg, The SAM-
TEX Team, Area selection for diamonds using magnetotellurics: Exam-
ples from Southern Africa, *Lithos* 112 (Supplement 1) (2009) 83 – 92.
doi:10.1016/j.lithos.2009.06.011.
- [24] D. Avdeev, A. Avdeeva, 3d magnetotelluric inversion using a limited-
memory quasi-newton optimization, *Geophysics* 74 (3) (2009) F45–F57.
doi:10.1190/1.3114023.
- [25] A. Avdeeva, M. Moorkamp, D. Avdeev, M. Jegen, M. Mienso-
pust, Three-dimensional inversion of magnetotelluric impedance tensor data and full
distortion matrix, *Geophysical Journal International* 202 (1) (2015) 464–
481.
- [26] R. Brown, T. Gernon, J. Stiefenhofer, M. Field, Geological constraints on
the eruption of the Jwaneng Centre kimberlite pipe, Botswana, *Journal of
Volcanology and Geothermal Research* 174 (1) (2008) 195–208.
- [27] F. Kolawole, E. A. Atekwana, S. Malloy, D. S. Stamps, R. Grandin,
M. G. Abdelsalam, K. Leseane, E. M. Shemang, Aeromagnetic, gravity,
and differential interferometric synthetic aperture radar analyses reveal
the causative fault of the 3 April 2017 mw 6.5 Moiyabana, Botswana,

420 earthquake, *Geophysical Research Letters* (2017) n/a–n/a/2017GL074620.
421 doi:10.1002/2017GL074620.

422 [28] S. Fishwick, Surface wave tomography: Imaging of the lithosphere-
423 asthenosphere boundary beneath central and southern Africa?, *Lithos*
424 120 (1-2) (2010) 63–73.

425 [29] F. Le Pape, A. G. Jones, J. Vozar, W. Wenbo, Penetration of crustal melt
426 beyond the Kunlun Fault into northern Tibet, *Nature Geoscience* 5 (5)
427 (2012) 330.

428 [30] M. Unsworth, S. Rondenay, Mapping the distribution of fluids in the crust
429 and lithospheric mantle utilizing geophysical methods, in: *Metasomatism*
430 *and the Chemical Transformation of Rock*, Springer, 2013, pp. 535–598.

431 [31] C. K. Rao, A. G. Jones, M. Moorkamp, The geometry of the Ia-
432 petus Suture Zone in central Ireland deduced from a magnetotelluric
433 study, *Physics of the Earth and Planetary Interiors* 161 (2007) 134–141.
434 doi:10.1016/j.pepi.2007.01.008.

435 [32] W. Heise, S. Ellis, On the coupling of geodynamic and resistivity models: a
436 progress report and the way forward, *Surveys in Geophysics* 37 (1) (2016)
437 81–107.

438 [33] O. Ritter, U. Weckmann, T. Vietor, V. Haak, A magnetotelluric study
439 of the Damara belt in Namibia: 1. regional scale conductivity anomalies,
440 *Physics of the Earth and Planetary Interiors* 138 (2) (2003) 71–90.

441 [34] U. Weckmann, Making and breaking of a continent: Following the scent
442 of geodynamic imprints on the African continent using electromagnetics,
443 *Surveys in Geophysics* 33 (1) (2012) 107–134.

444 [35] M. P. Miensoopust, A. G. Jones, M. R. Muller, X. Garcia, R. L. Evans,
445 Lithospheric structures and Precambrian terrane boundaries in northeast-
446 ern Botswana revealed through magnetotelluric profiling as part of the

- 447 Southern African Magnetotelluric Experiment, *Journal of Geophysical Re-*
448 *search: Solid Earth* 116 (B2).
- 449 [36] R. Hyndman, P. Shearer, Water in the lower continental crust: modelling
450 magnetotelluric and seismic reflection results, *Geophysical Journal Inter-*
451 *national* 98 (2) (1989) 343–365.
- 452 [37] M. Becken, O. Ritter, P. Bedrosian, U. Weckmann, Correlation between
453 deep fluids, tremor and creep along the central san andreas fault, *Nature*
454 480 (7375) (2011) 87–90.
- 455 [38] M. Becken, O. Ritter, Magnetotelluric studies at the san andreas fault zone:
456 implications for the role of fluids, *Surveys in Geophysics* 33 (1) (2012) 65–
457 105.
- 458 [39] D. Hasterock, The global heat flow database of the international heat flow
459 commission, <http://www.heatflow.und.edu/index2.html>.
- 460 [40] A. Schaeffer, S. Lebedev, Global shear speed structure of the upper mantle
461 and transition zone, *Geophysical Journal International* 194 (1) (2013) 417–
462 449.
- 463 [41] S. Ballard, H. N. Pollack, N. J. Skinner, Terrestrial heat flow in botswana
464 and namibia, *Journal of Geophysical Research: Solid Earth* 92 (B7) (1987)
465 6291–6300. doi:10.1029/JB092iB07p06291.
- 466 [42] R. L. Evans, A. G. Jones, X. Garcia, M. Muller, M. Hamilton, S. Evans,
467 C. Fourie, J. Spratt, S. Webb, H. Jelsma, et al., Electrical lithosphere
468 beneath the Kaapvaal craton, southern Africa, *Journal of Geophysical Re-*
469 *search: Solid Earth* 116 (B4).
- 470 [43] A. G. Jones, J. Ledo, I. J. Ferguson, C. Farquharson, X. Garcia, N. Grant,
471 G. McNeice, B. Roberts, J. Spratt, G. Wennberg, et al., The electrical
472 resistivity structure of Archean to Tertiary lithosphere along 3200 km of
473 SNORCLE profiles, northwestern Canada, *Canadian Journal of Earth Sci-*
474 *ences* 42 (6) (2005) 1257–1275.

- [44] K. Selway, Electrical discontinuities in the continental lithosphere imaged with magnetotellurics, in: H. Yuan, B. Romanowicz (Eds.), *Lithospheric Discontinuities*, John Wiley & Sons, Inc, 2019, pp. 89–109.
- [45] M. M. Hirschmann, Water, melting, and the deep earth h₂o cycle, *Annu. Rev. Earth Planet. Sci.* 34 (2006) 629–653.
- [46] A. Zunino, A. Khan, P. Cupillard, K. Mosegaard, *Constitution and Structure of Earth’s Mantle*, John Wiley & Sons, Inc, 2016, pp. 219–243. doi:10.1002/9781118929063.ch11. URL <http://dx.doi.org/10.1002/9781118929063.ch11>
- [47] A. G. Jones, Proton conduction and hydrogen diffusion in olivine: an attempt to reconcile laboratory and field observations and implications for the role of grain boundary diffusion in enhancing conductivity, *Physics and Chemistry of Minerals* 43 (4) (2016) 237–265.
- [48] S. Fishwick, A. Reading, Anomalous lithosphere beneath the proterozoic of western and central australia: a record of continental collision and intraplate deformation?, *Precambrian Research* 166 (1-4) (2008) 111–121.
- [49] S. Lebedev, J. Boonen, J. Trampert, Seismic structure of precambrian lithosphere: New constraints from broad-band surface-wave dispersion, *Lithos* 109 (1-2) (2009) 96–111.
- [50] H. Pedersen, S. Fishwick, D. Snyder, A comparison of cratonic roots through consistent analysis of seismic surface waves, *Lithos* 109 (1-2) (2009) 81–95.
- [51] T. Eeken, S. Goes, H. A. Pedersen, N. T. Arndt, P. Bouilhol, Seismic evidence for depth-dependent metasomatism in cratons, *Earth and Planetary Science Letters* 491 (2018) 148–159.
- [52] K. Selway, H. Ford, P. Kelemen, The seismic mid-lithosphere discontinuity, *Earth and Planetary Science Letters* 414 (2015) 45–57.

- [53] D. Wang, Y. Guo, Y. Yu, S.-i. Karato, Electrical conductivity of amphibole-bearing rocks: influence of dehydration, *Contributions to Mineralogy and Petrology* 164 (1) (2012) 17–25. doi:10.1007/s00410-012-0722-z.
- [54] U. H. Faul, I. Jackson, The seismological signature of temperature and grain size variations in the upper mantle, *Earth and Planetary Science Letters* 234 (1) (2005) 119–134.
- [55] K. Selway, Negligible effect of hydrogen content on plate strength in East Africa, *Nature Geoscience* 8 (7) (2015) 543.
- [56] D. Bercovici, Y. Ricard, Mechanisms for the generation of plate tectonics by two-phase grain-damage and pinning, *Physics of the Earth and Planetary Interiors* 202 (Supplement C) (2012) 27 – 55. doi:<https://doi.org/10.1016/j.pepi.2012.05.003>.
- [57] R. Vissers, M. Drury, E. Hoogerduijn, C. Spiers, D. Van der Wal, et al., Mantle shear zones and their effect on lithosphere strength during continental breakup, *Tectonophysics* 249 (3-4) (1995) 155–171.
- [58] P. Wessel, W. H. Smith, New, improved version of the generic mapping tools released, *EOS Trans. AGU* 79 (1998) 579.

Acknowledgements

All magnetotelluric data used in this study can be downloaded from <http://www.complete-mt-solutions.com/mtnet/data/samtex/samtex.html>. The surface wave model was generated using seismic waveform data are available from the seismic data centres, IRIS and GEOFON Potsdam. Where waveform data are not currently open access (due to a moratorium following deployment) principal investigators of the seismic experiments should be contacted (see below for information).

527 The authors wish to acknowledge the tremendous contribution made to this
 528 work by all those people involved in the numerous deployments for seismolog-
 529 ical and magnetotelluric data acquisition across southern Africa. In addition
 530 to the funding and logistical support provided by SAMTEX consortium mem-
 531 bers (Council for Geoscience, Geological Surveys Botswana and Namibia, De
 532 Beers Group Services, Rio Tinto Exploration, and BHP Billiton), this work was
 533 also supported by research grants from National Science Foundations Continen-
 534 tal Dynamics program (USA, EAR0309584 and EAR0455242), the Department
 535 of Science and Technology (South Africa), and Science Foundation Ireland (Ire-
 536 land, grant 05/RFP/GEO001). We also thank the many farmers and landowners
 537 in Botswana, Namibia, and South Africa for their voluntary cooperation in al-
 538 lowing the deployment of MT stations on their properties. Seismic data has been
 539 accessed from the IRIS data management centre, and GFZ Potsdam. Particu-
 540 lar thanks are given to Cindy Ebinger, Georg Ruempker and Donna Shillington
 541 for access to data that was not publically available at the time of preparation.
 542 Figures 1, 2, 6 and 7 are plotted using the Generic Mapping Tools[58]. This re-
 543 search used the ALICE High Performance Computing Facility at the University
 544 of Leicester. Finally, we would like to than E. Calais, an anonymous reviewer
 545 and the editor J. Brodholt for their comments that improved the quality of the
 546 manuscript.